Side Chain and Flexibility Contributions to the Raman Optical Activity Spectra of a Model Cyclic Hexapeptide

Jana Hudecová,[†,‡] Josef Kapitán,[†] Vladimír Baumruk,[‡] Robert P. Hammer,[§] Timothy A. Keiderling,*[,∥] and Petr Bouř*[,†]

Institute of Organic Chemistry and Biochemistry, Academy of Sciences, Flemingovo nám. 2, Prague 6, 16610, Czech Republic, Institute of Physics, Charles University, Ke Karlovu 5, 12116, Prague 2, Czech Republic, Department of Chemistry, Louisiana State University, 232 Choppin Hall, Baton Rouge, Louisiana 70803-1804, and Department of Chemistry, University of Illinois at Chicago, 845 West Taylor Street, Chicago Illinois 60607-7061

Received: May 24, 2010; Revised Manuscript Received: June 10, 2010

A model peptide, cyclo-(Phe-D-Pro-Gly-Arg-Gly-Asp), with a distinct folded structure containing short β-hairpin and β-sheet patterns was studied by Raman and Raman optical activity (ROA) spectroscopies. Unlike for previously analyzed vibrational circular dichroism of the same compound (*Chirality* **2008**, *20*, 1104), the Raman spectrum is dominated by side chain contributions and is more sensitive to their geometry fluctuations. The spectra and molecular motion were analyzed with the aid of the density functional theory simulations combined with molecular dynamics (MD). The side chain geometry fluctuations were found to significantly contribute to the broadening of the spectral bands, while dynamics of the backbone is rather restricted. According to our MD results, the side chains do not move freely but largely oscillate around preferred conformations. Averaging of computed spectra for many structures derived from the MD trajectories provided better spectral profiles than did a fixed geometry. The Raman and ROA scattering is dominated by the more polarizable phenylalanine and proline groups, as could be verified both by the computations and by comparison to experiments with a model Phe-D-Pro dipeptide. Computational analyses suggest that the ROA spectrum mostly senses local side chain conformation, whereas a vibrational coupling between different side chains contributes less. The coupling is mostly mediated by the peptide backbone and is restricted to specific vibrational region. The ROA spectroscopic technique thus provides important local structural information that needs, however, to be extracted by multiscale (QM/MM) simulation techniques.

Introduction

Chiral spectroscopy has become a standard means of conformational analyses of peptide structures. For example, α-helices yield a characteristic electronic circular dichroism (ECD) signal that can be used to determine the helical contents in peptides and proteins[1−3] or to study chiral interactions of aromatic amino acid residues.[4] Vibrational circular dichroism (VCD) is particularly sensitive to the main chain conformation, and studies of amide-centered vibrational modes that are coupled in the chain provide even more reliable discrimination between repeating secondary structures, such as α-helices, 3_{10}-helices, and β-sheet and coil conformations.[5−8] Finally, Raman optical activity (ROA) spectra bear similar information as VCD, but the signal comes from many different modes sampling all aspects of the peptide molecules, especially the aromatic side chains.[9−11]

Monitoring of more local and chain conformation is problematic. Sites such as peptide β-hairpins contribute relatively weakly to the overall spectral response. In some cases, they can be discriminated by labeling with stable isotopes and identified in the IR and VCD spectra.[12−16] Structural fluctuations lead to complex perturbations of the spectra and difficulties in interpretation. Some peptides can be induced to have relatively stable structures, such as the Ala-rich α-helical models,[17] Aib-containing 3_{10} helices,[18] high Pro content 3_1-helices,[19] and hydrophobically or turn-stabilized β-hairpins.[20−23] As another option, modeling small structural elements with cyclic peptides enables one to study specific peptide segments on a conformationally restricted system that is accessible to relatively precise computations.[23−25] In the past we used the cyclo-(Phe-D-Pro-Gly-Arg-Gly-Asp) molecule to investigate the structure, flexibility, and the IR and VCD spectral components related to the β-turn induced by the D-Pro-Gly moiety.[26] The type I′ turn was determined as the most reasonable conformation of this sequence, although the peptide exhibited unexpected flexibility that caused a broadening of the spectral bands. However, no information about the side chain conformation was obtained from its IR and VCD spectra.

In this study, we analyze the Raman and ROA spectra of this peptide, and use quantum chemical spectral simulations to determine the link between the spectral shape and the structure. Unlike for VCD, Raman and ROA spectra are dominated by the scattering from the bulky polarizable residues, here in particular the phenylalanine and proline. Although for small peptides exact conformer ratios can be obtained from the ROA spectrum,[27] for larger ones an inhomogeneous line broadening and multiconformational equilibrium complicate the analysis.[28,29] As shown below, relatively robust computational techniques had to be used for the cyclopeptide. Nevertheless, we were able to assign most of the observable Raman bands and to determine

* To whom correspondence should be addressed, tak@uic.edu (T.A.K.) and bour@uochb.cas.cz (P.B.).
[†] Academy of Sciences.
[‡] Charles University.
[§] Louisiana State University.
[∥] University of Illinois at Chicago.

10.1021/jp104744a
Published on Web 06/28/2010

the mechanisms from which the inelastic scattering optical activity of the cyclopeptide originates.

Density functional theory (DFT) computations provide a practical way for interpretation of peptide vibrational spectra. Estimation of the ROA tensors would be sufficient on the HF level; however, force fields that are sufficiently accurate for vibrational optical activity computations require inclusion of the correlation energy.[30] The first DFT computations of ROA were based on a rather lengthy numerical differentiation of the intensity tensors.[31] Lately more analytical algorithms allowed one to determine ROA on a similar time scale as for the Raman intensities.[32,33] This enabled us to directly simulate the spectra for several structures obtained as MD snapshots. However, for large molecular systems or in order to average spectra of many (thousand) conformers, it is more practical to transfer vibrational properties (the intensity and force field tensors) from a small library of precalculated fragments or structures.[34,35] In this study, the latter approximate computation proved useful for qualitative modeling of peptide dynamics and its effect on the Raman line broadening.

Methods

Experimental Section. The cyclo-(Phe-D-Pro-Gly-Arg-Gly-Asp) hexapeptide was synthesized on an ABI Pioneer peptide synthesizer and was described in detail elsewhere.[26] The cyclic protocols took advantage of three-dimensional orthogonal protection schemes[36] based on base-labile Fmoc, acid-labile (TFA) side-chain group, and allyl (Al) groups, which are piperidine and TFA-stable and removed with Pd(0) catalysts. This scheme for on-resin synthesis of backbone amide and side-chain amide cyclized peptides was first systematically described by Barany, Kates, and Albericio.[37] Additionally, a shorter peptide sequence was also studied experimentally, as the Phe-D-Pro dipeptide (HCl salt), purchased from Bachem (G-3355) and refined by HPLC.

The hexapeptide was dissolved in deionized water (4.4 mg in 80 μL, ~0.09 mol/L) and filtered through a 0.22 mm Millipore filter into a quartz cell, which provided a positively charged peptide form. The dipeptide compound was measured at pH = 1 (no pH adjustment, at a concentration of 1 mol/L) and pH = 13 (using NaOH to adjust pH, so that the peptide concentration dropped to ~0.8 mol/L). Measurement at pH = 7 was lost due a calibration error and not repeated due to a shortage of purified sample; nevertheless preliminary Raman spectra did not indicate significant differences from the other dipeptide charged forms, which is important for the comparison with the hexapeptide.

Raman optical activity and Raman scattering spectra of all samples were recorded on ROA spectrometer built at the Institute of Physics of the Charles University,[38] which uses a backscattering geometry with incident circular polarization (ICP) modulation. Experimental conditions were as follows: excitation wavelength 514.5 nm, laser power at the sample 434 mW (for hexapeptide) or 535 mW (for Phe-D-Pro), spectral resolution ~6.5 cm^{-1}, acquisition time 35.5 (hexapeptide) and 15 hours (Phe-D-Pro). The solvent signal was subtracted from the sample Raman spectra, and minor baseline corrections were made. Raw measured ROA spectra were Fourier filtered to suppress a quasi-periodic high-frequency CCD signal in the low wavenumber region, corrected for spurious artifact signal from solvent and cell walls, and slightly baseline corrected. The ROA signal close to 1003 cm^{-1} is probably not reliable because of a highly polarized Raman band situated in this region.

Molecular Dynamics (MD) Conformational Studies. The simulations for the protonated hexapeptide (which is relevant to the acidic experimental conditions) were performed using the Tinker program package.[39] The Amber95[40,41] force field was used with periodic boundary conditions (box 30 Å), NpT ensemble, 1 fs integration time step, and a pressure of 1 atm. Simulated annealing (from 1000 to 300 K, 1 ns) was followed for 5 ns in a production run at 300 K. Significant backbone conformational changes were not observed, even at the elevated temperatures; however, for the side chains a reasonable equilibrium conformer distribution could be obtained as they could rotate many times during the simulation. Snapshots used for the approximate spectral simulations were saved every 1 ps. For the ab initio computations, 26 conformers were selected by sampling every 200 ps from the same trajectories.

Quantum-Chemical Computations. The Gaussian software, versions 03[42] and 09,[43] was used for energy minimization and the spectral parameter generation. Geometries of the 26 selected conformers were optimized using the constrained normal mode method.[44,45] Modes with energies within i300(imaginary)−300 cm^{-1} were fixed, which had approximately the same effect on geometry as more common torsion angle restraints. With normal modes, the higher-frequency vibrational coordinates, those most important for the observed spectra, could be relaxed with a minimal impact on the conformation obtained in the MD determined structure. For optimized geometries the force fields (FF), polarizability (α), and optical activity tensors[46] ($\mathbf{G}'$, $\mathbf{A}$) were calculated. The BPW91[47] and B3LYP[48] functionals, standard 6-31G** basis set, and COSMO[49] solvent correction (its Gaussian version is denoted as CPCM) were used by default. The spectral intensities were convoluted with Lorentzian bands 8 cm^{-1} wide and multiplied by a Boltzmann factor for 300 K to account for scattering from excited vibrational levels.[50,51]

Approximate Conformational Averaging of Spectra. To estimate the effect of the dynamics for a larger set of conformers, the Cartesian coordinate transfer (CCT)[34] of force field and intensity tensors onto the 1 ps snapshot geometries was used to generate the spectra. By the algorithm described elsewhere[35] the tensors were transferred from the 26 conformations mentioned above on the MD snapshots, using a local similarity in structures of the source and target geometries as a criterion for the transfer.

Results and Discussion

Hexapeptide Structure and Dynamics. Our 5 ns trajectory was too short to provide equilibrium backbone conformer distribution. Nevertheless, previous MD runs with longer times and different force fields provided the same backbone conformer, which was also found to be consistent with analysis of the VCD spectra.[26] That the high-temperature phase does not affect the conformation suggests a high stability of the folded cyclic peptide backbone as well, at least within the Amber force field model. Thus, in this study, we take the backbone structure from our previous MD study and concentrate here on the side chain motion. The D-Pro-Gly2 sequence in the hexapeptide maintained the starting a type I′ β-turn ($\varphi_2 \sim 60°$, $\psi_2 \sim 30°$, $\varphi_3 \sim 90°$, and $\psi_3 \sim 0$, see Figure 1 for the torsion angle definition) in the simulations. Transitions to a type II′ ($\varphi_2 = 60°$, $\psi_2 = -120°$, $\varphi_3 = -90°$, and $\Psi_3 = 0°$) turn are not probable at room temperature.[26]

The side chain angles fluctuate more than the backbone parameters. Their temporal changes (1000 → 300 K during 1 ns annealing followed by a 5 ns run at 300 K) and MD distributions (300 K only) are represented in the angular

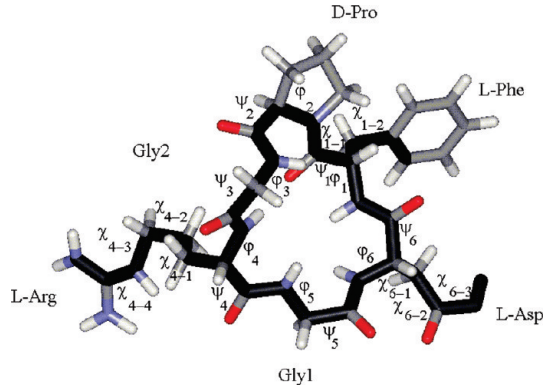

Figure 1. The cyclic hexapeptide and definition of main torsion angles.

distribution plot in Figure 2. The χ_{1-1} angle of Phe mostly adopts values around 60°, −60°, and 180° are less probable, although the MD propagation time may not be sufficient to obtain a converged equilibrium distribution. The χ_{1-2} angle oscillates exclusively around −90° and 90°, which corresponds to the same geometry due to the phenyl symmetry. The Arg χ_{4-1}, χ_{4-2}, χ_{4-3}, χ_{4-4} angles oscillate around −60°, 180°, and 60°, the canonical rotamer values, with a strong preference for 180° except for χ_{4-4}, which is relatively evenly distributed in the −180 to −60° and 60 to 180° intervals. The angle χ_{6-1} of Asp has a strong preference for −170 and −60°, while χ_{6-2} is largely dispersed, mostly around 90°, and χ_{6-3} fluctuates near 0°.

Ab Initio Models for Spectral Intensities. Previous studies reported that ROA calculations had various degrees of sensitivity to the electronic model used, according to the investigated systems.[31,52−54] For an arbitrarily selected MD conformer of the hexapeptide, we have estimated the Raman and ROA spectra using the 6-31G, 6-31G**, and 6-31++G** basis sets with the B3LYP functional, and again from the BPW91 and B3LYP functionals with the 6-31G** basis set as compared in Figure 3. The 6-31G basis provides similar Raman, but rather different ROA intensities, if compared to the 6-31G** and 6-31++G** results. Adding diffuse functions (++) to the basis does not change the basic relative intensity and ROA sign patterns, although notable differences are apparent throughout the entire spectral region. Allowing for basis set dependent frequency shifts, there is much more similarity than dissimilarity in those three basis set varying spectra, both Raman and ROA. For the most part signs and relative intensities are in agreement.

As expected, the ROA intensities are more sensitive to the basis set variation. In particular, within 400−600 cm^{-1} the simulated sign pattern does not seem to converge. This does not affect comparison with experiment, where only the region within ~800 to 1800 cm^{-1} could be measured reliably; the signal below 800 contains contribution from water that cannot be fully interpreted with the continuum solvent model. Larger basis sets

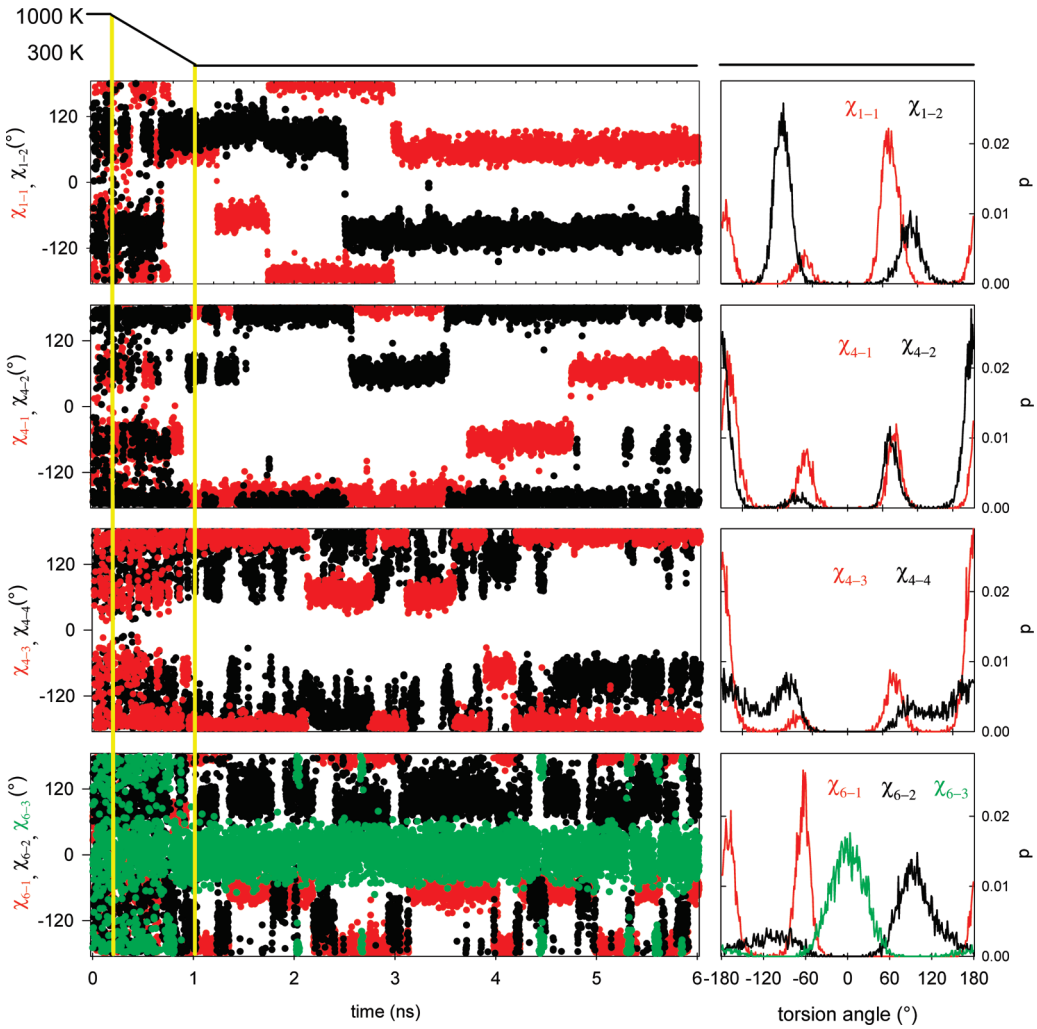

Figure 2. The time dependence (left) and distribution (right) of the side chain torsion angles in the hexapeptide obtained by MD. Amber 95 force field was used; the distributions do not include the 1000 K equilibration and 1000 → 300 K annealing phases.

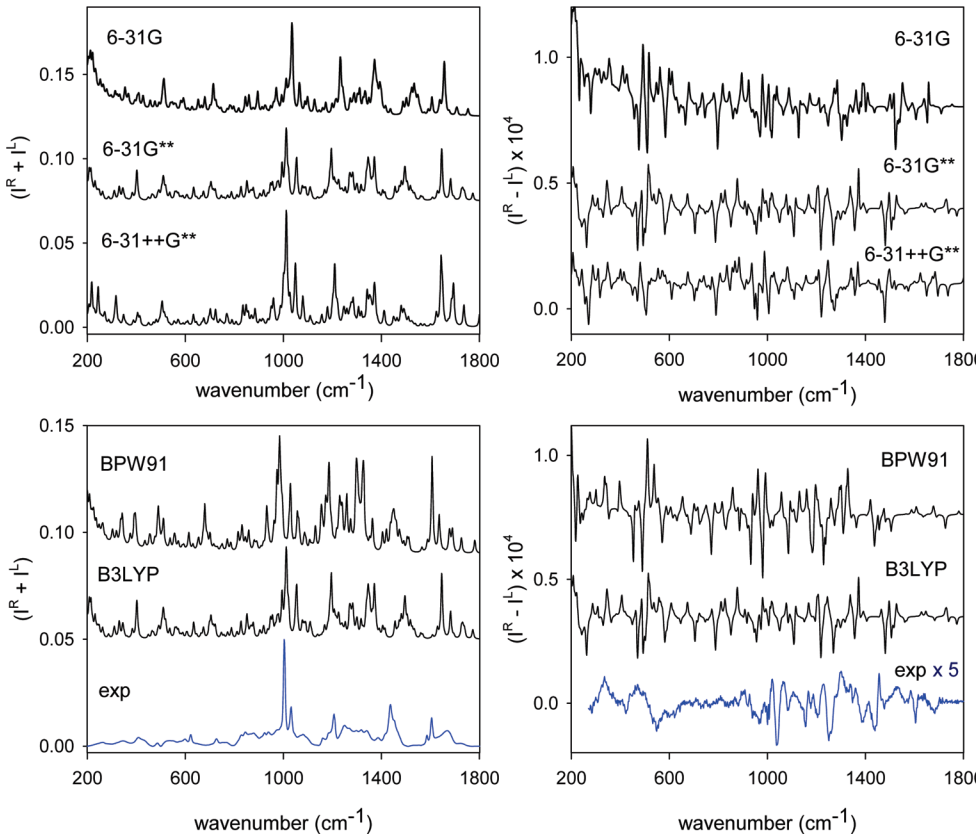

Figure 3. (Top, for B3LYP/CPCM) Basis and (bottom, for 6-31G**) functional dependence of (left) Raman and (right) ROA hexapeptide spectra.

than 6-31++G** are not feasible for ROA calculations of the cyclopeptide; but in previous tests they did not bring a significant improvement for predicted spectra of smaller systems.[54]

Inclusion of the solvent explicitly for the ROA calculations is currently not possible as the hydrated peptide size and the CPU time would grow beyond our computational possibilities. Additionally, previous results suggest that a large number of geometries (water configurations) is needed to average the water contribution to ROA.[55,56] However, the influence of individual water molecules is partially accounted for in the molecular dynamics, where they stabilize the cyclopeptide conformation. We thus suppose that the main ROA pattern stems from the molecular structure of the peptide and is not significantly modified by hydrogen bonds to water molecules, only partially represented by the implicit solvent model.

The BPW91 GGA functional has been previously used for peptide VCD computations,[57,58] since it provides realistic amide I (C═O stretching, ∼1650 cm^{-1}) frequencies for lower computational cost. However, the B3LYP hybrid method (containing the HF exchange) has been previously shown to be more suitable for Raman studies that comprise a larger wavenumber region.[55] Typically, BPW91 frequencies are too low below 1200 cm^{-1}, if compared with experiment. On the other hand, the B3LYP frequencies are much too high for higher wavenumber modes, particularly those associated with the amide linkage. This can be observed also for the hexapeptide (Figure 3, bottom). Additionally, the Raman relative intensity pattern seems to be better predicted by B3LYP. Note, however, that the one-conformer simulation is not directly comparable to the experiment; for ROA, for example, the experimental intensities (multiplied by 5 in Figure 3) are much smaller than the calculated ones, due to the averaging described below. Because of this comparison and our previous experience, we chose to use B3LYP; for the hexapeptide its computational cost is only slightly higher (by ∼50%) than that of BPW91. On the other hand, the diffuse basis 6-31++G** makes the computations much longer than those obtained with 6-31G**; therefore the smaller 6-31G** basis was used for the conformer averaging calculations.

Part of the ROA intensities stems from magnetic dipole and electric quadrupolar parts, which can contain some contributions from the electric dipolar polarizability, dependent on the choice of the coordinate origin.[46] In the past a polarization model, neglecting the magnetic and electric quadrupolar contributions irreducible by a coordinate transformation, was proposed as a versatile tool for approximate spectral computations.[55,59−61] For the hexapeptide, we can see (Figure 4) that the polarization model correctly reproduces almost all the full quantum computed ROA signs and relative intensity patterns. Approximate intensities can thus be obtained with a lower computational cost, although the latest fast analytical ROA simulation methods[32,33] made this advantage less significant. This demonstration that the intrinsic magnetic contribution is of quite small impact also enables us to interpret the vibrational optical activity primarily as a result of vibrational coupling between polarizable molecular moieties,[46] although these may not be associated with usual chromophore groups.

Conformational Averaging. The one-conformer Raman and ROA spectra (for example, see Figure 3) only approximately matched the experiment. Many features could be made more realistic if the spectra of many conformers are averaged. This can be seen in Figure 5, where the average of 5000 conformers obtained by the CCT transfer and that of 26 conformers whose spectra were computed ab initio are compared to the experimental Raman and ROA intensities. For easier assignment and comparison, scaled simulated spectra were also created and

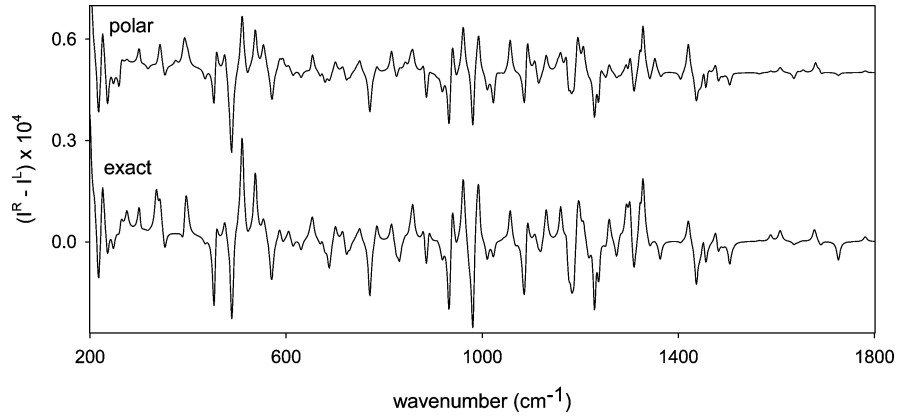

Figure 4. Comparison of the polarization and exact ROA computational models, on the hexapeptide BPW91/6-31G** spectra.

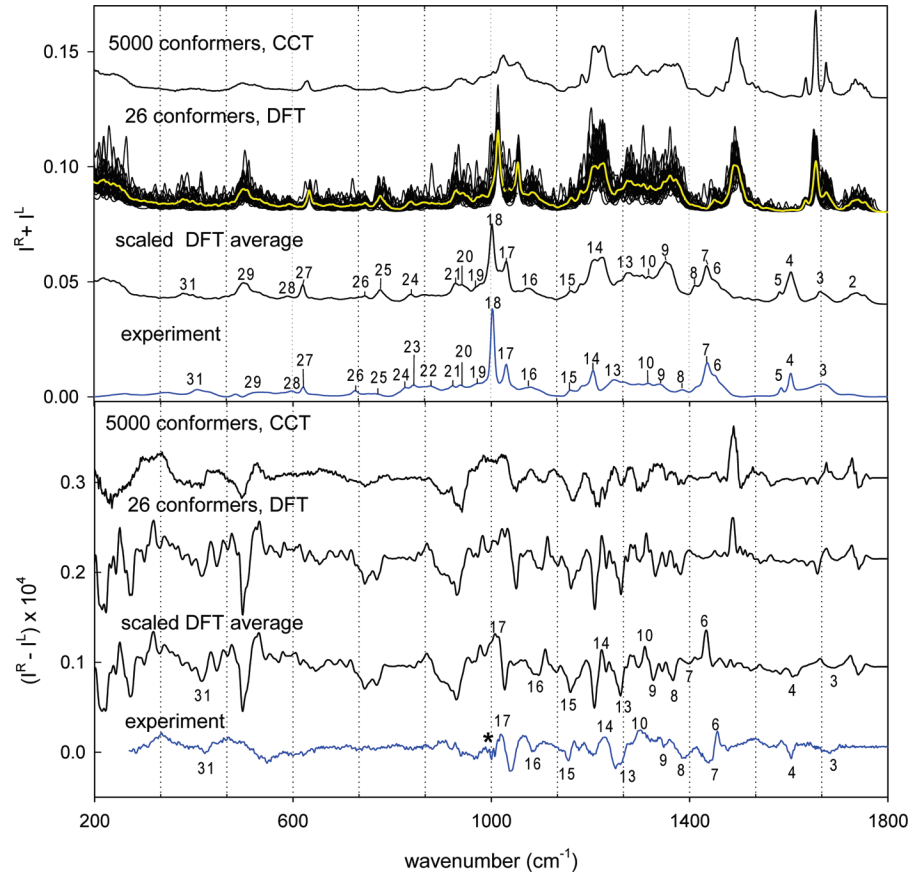

Figure 5. Conformational averaging of the Raman ($I^R + I^L$) and ROA ($I^R - I^L$) hexapeptide spectra. As indicated, 5000 MD structures were averaged with the CCT method and the DFT (B3LYP/CPCM/6-31G**) results of 26 conformers were averaged directly, scaled, and compared to experiment. The asterisk (*) marks the experimental ROA part that might be affected by a strongly polarized 1003 cm^{-1} Raman band. The band numbers correspond to the assignments in Table 1.

displayed in Figure 5. For the scaling we used our own software;[62] simulated bands were aligned with the experimental ones (cf. the assignment in Table 1), common scale factors were used for all 26 conformers, but computed order of the vibrational frequencies was not changed. The averaging, in particular that based on the ab initio structures, dramatically improves shape and intensity distribution of the Raman spectrum. Typically, signals arising from the polar groups (C═O stretch, at ∼1670 cm^{-1}, arginine N−H bending, and aspartate C═O stretching vibrations) are dispersed, but also bending vibrations of the hydrophobic CH groups (∼1200−1450 cm^{-1}) coalesce into a broader but not monotonic profile. Only peaks associated with the phenyl ring vibrations (e.g., at 621, 1003, 1033, 1207, and 1605 cm^{-1}) remain relatively sharp.

By contrast, the CCT averaging of spectra for 5000 snapshot structures (see top Raman spectrum, Figure 5) leads to bands that are too broad, in particular those at 1003 and 1033 cm^{-1}, which can be attributed to the approximations associated with the transfer, as well as to inaccuracy and neglecting of the quantum effects in the Amber force field averaging. However, the other bands are in reasonable agreement with the unscaled ab initio shapes (frequencies were not shifted).

Unlike for Raman, the averaging does not provide band-to-band correspondence between the calculated and experimental ROA spectra (Figure 5, bottom), although especially within 1000−1800 cm^{-1} a majority of bands can be identified on the basis of the right sign and relative intensity agreement. The disagreement between the theoretical and experimental 1437

TABLE 1: Calculated and Experimental Frequencies (cm^{-1}) of Most Intense Raman/ROA Hexapeptide Bands and the Vibrational Mode Assignment

band	ω_{cal}, CPCM/6-31G** B3LYP	BPW91	ω_{exp}	vibration[a]
1	1773	1726	1727	ν(CO), Asp
2	1731	1690	1690	AI, Pro, Gly
3	1683	1636	1669	AI, Pro
4	1646	1607	1605	Phe, ν(C=C)
5	1629	1589	1586	Phe, ν(C=C)
6	1534	1473	1453	Phe, ν(C=C)
7	1496	1451	1437	AII, C−H sciss., Pro δ($^{\alpha}$C−H)
8	1406	1364	1388	AII, Pro, δ($^{\alpha}$C−H)
9, 10	1344, 1371	1297, 1327	1319, 1340	Phe + Pro, δ(CH)
11, 12	1283, 1301	1233, 1259	1270, 1298	AII, Gly; CH_2 twist
13	1280	1230	1249	Pro, Phe, δ(CH)
14	1196	1186	1207	Phe, δ(CH)
15	1168	1155	1160	Asp, ν(C−CO); Phe δ(CH)
16	1090	1057, 1087	1080	ν(C−N), ν(C−C)
17	1054	1029	1033	Phe breathing, ν(C=C), Pro ν(C−C)
18	1012	985	1003	Phe breathing ν(C=C), deloc. ν(C^{α}−C)
19−25	820−995	815−974	827−966	Phe δ(C−H) oop, ν(C−C)
26	704	679	726	(C=O) oop
27	634	614	621	Phe def.
28	604	608	599	Phe def., deloc.
29	510	510	538	Phe NH oop
30	464	488	485	deloc, Arg NH oop
31	402	395	408	Pro def.

[a] Key: oop, out of plane; AI, amide I; AII, amide II.

cm^{-1} ROA band is rather an exception in this region. Below 1000 cm^{-1}, the relatively intense ROA simulated signal for the 26 conformers suggests that more structures need to be taken to obtain a converged signal. Indeed, the CCT 5000 structure averaging provided less intensity in the low-frequency region. Within 700−1800 cm^{-1} the 5000 conformer CCT and the 26 conformer DFT average ROA spectra are reasonably close, which suggests a more constrained effect of peptide motion on these higher-energy vibrations. Although we may expect some inaccuracies introduced by the transfer method, these do not seem to be a limiting factor at the current level of accuracy.

The averaging also leads to much lower (~5×) ROA/Raman intensity ratios, yielding values more comparable to experiment. Such strong ROA intensity decrease was not observed before in similar calculations for regular polyproline chain.[61] It nevertheless qualitatively corresponds to effects expected from the large side chain flexibility predicted by MD (Figure 2). The time-averaged local chirality of these side chains is thus smaller than that of well-defined conformers, much as seen previously for a flexible sugar compound.[63] A detailed comparison of the scaled ROA spectra and experiment nevertheless reveals many shape similarities, namely, in the higher-frequency (~1000−1800 cm^{-1}) region. Apart of the limited accuracy of the experiment and simulation, the differences in the calculated and experimental intensities reflect the high sensitivity of ROA to details of molecular geometry.

Single Residue Signals and the Phe-D-Pro Dipeptide Example. To develop some concept for the contribution of individual amino acids to the computed spectral intensities, we simulated the hexapeptide spectra at the B3LYP/CPCM/6-31G** level for an arbitrary conformer, but with the intensity tensors[46] set to zero, except for a selected residue, as shown in Figure 6. Clearly, the phenylalanine dominates the spectrum, but the difference is less dramatic for ROA, where the D-Pro, Arg, and Asp residues all contribute significantly. Nevertheless, we suppose that the arginine and aspartate contribution to the experimental spectra will be less significant than that in the simulated spectrum, because of its strong interaction with the solvent and consequent band broadening. Yet, for ROA, we see that a significant part of the signal simulated for the full peptide cannot be reconstructed as a sum of the amino acid components. Some bands (e.g., the 1207 cm^{-1} on of Phe CH bending) can be almost up to 100% modeled by the sum, whereas for some, in particular below 1000 cm^{-1}, the local contribution to ROA intensity is quite minor. The short-distance

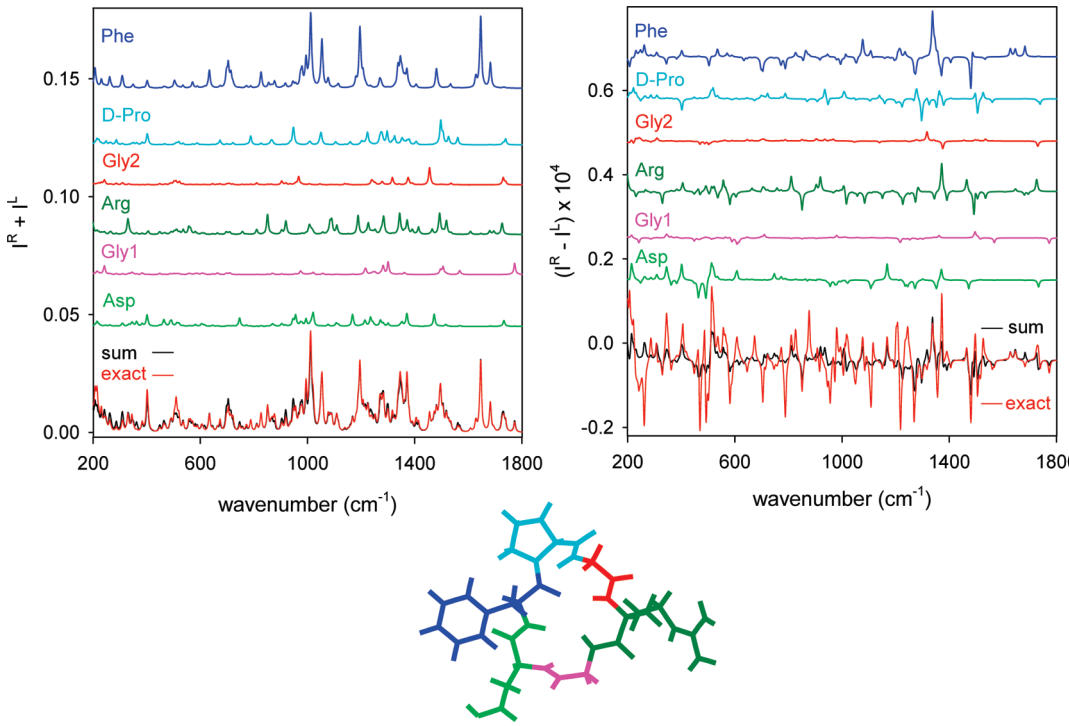

Figure 6. Simulated (B3LYP/CPCM/6-31G**, one conformer) hexapeptide Raman and ROA spectra (bottom, red) and approximate contributions of individual amino acid residues.

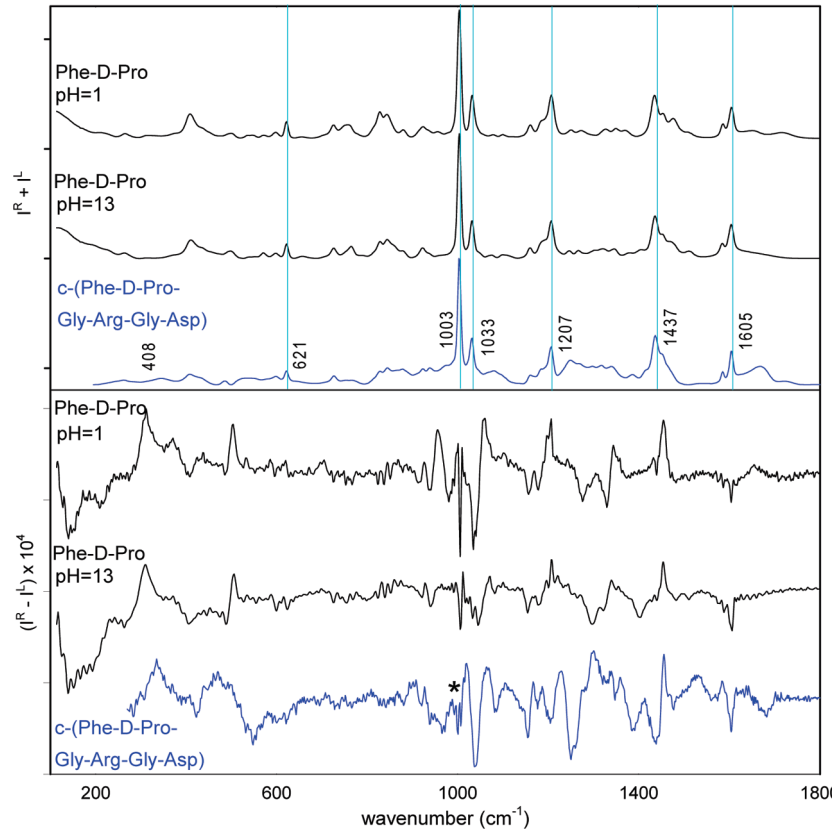

Figure 7. Experimental ROA (top) and Raman (bottom) spectra of the model Phe-D-Pro dipeptide (for pH = 1 and pH = 13), and those of the hexapeptide. The asterisk (*) marks experimental ROA part that might be affected by strongly polarized 1003 cm^{-1} Raman band.

coupling is thus at least as important for peptide ROA as the local chirality.

With such a dominating Phe contribution, it is therefore not surprising that the experimental Raman spectra of the Phe-D-Pro model compound resembles that of the hexapeptide (Figure 7). In particular the positions of the strongest Phe and Pro bands, which are weakly influenced by the solvent, are almost identical. The origin of the majority of the Raman signal in the more polarizable side chains is also indicated by the similarity of the protonated (pH = 1) and anionic (pH = 13) dipeptide spectra.

The correspondence between the dipeptide and hexapeptide ROA (Figure 7, top) is less clear. Below 900 cm^{-1}, the signal is strongly influenced by water,[55] and no features are directly comparable. However, within ~1000−1650 cm^{-1}, many spectral features are common which suggest that the ROA signal at those parts originates locally from the Pro and Phe residues, in both di- and hexapeptide.

To investigate the dependence of the ROA pattern on the local conformation, we performed a conformer scan in a simplified Phe-D-Pro fragment (Figure 8), scanning the angles χ_{1-1} and ω for both the north (N) and south (S) proline ring puckering.[55,64] In Table 2 the 18 lowest-energy conformers of the total of 36 are listed. The starting angles ψ were chosen, −60, 60, and 180°, and then allowed to relax freely from these starting geometries. As apparent from Table 2, the conformer changes are associated with rather small energies. In Figure 9, the effects of the proline puckering and ω and χ_{1-1} rotations on the ROA are simulated from averaged spectra over the other coordinates. The S and N proline forms, which are thought to be about equally populated in peptides and proteins,[55,61,65−68] lead to rather modest changes in the spectra and most probably cannot be detected in the hexapeptide due to the limited sensitivity. The C−H bending vibrations (~1350 cm^{-1}) most influenced by the puckering are significantly broadened by other motions in the hexapeptide (cf. Figure 5).

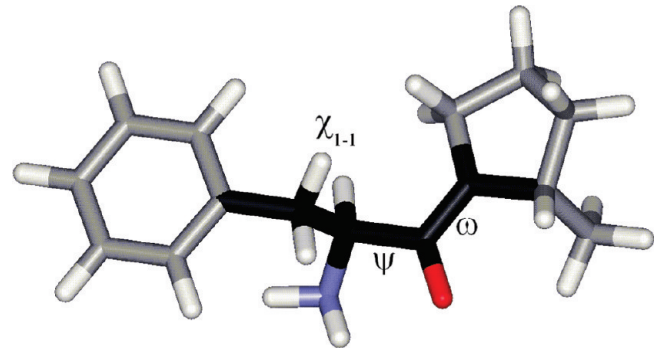

Figure 8. The Phe-D-Pro model fragment and the main the torsion angles.

TABLE 2: Dihedral Angles and Relative Conformer Energies (BPW91/CPCM/6-31G) of the Model Phe-D-Pro Fragment**

		N-Pro conformers		S-Pro conformers	
χ_{1-1} (deg)	ω (deg)	Ψ (deg)	E (kcal/mol)	Ψ (deg)	E (kcal/mol)
180	180	−96	0.3	−97	0.0
180	0	−113	0.7	−116	0.6
180	180	−171	1.3	−157	0.5
60	180	−114	1.1	−116	0.7
180	0	−129	1.6	−147	0.8
60	0	−134	2.3	−135	1.4
−60	180	−90	2.1	−87	1.7
60	180	−159	3.8	−117	0.8
−60	0	−104	3.1	−103	3.1

The cis−trans ω-isomerization (Figure 9) causes solitary sign changes mostly within 200−1000 cm^{-1}, but surprisingly the

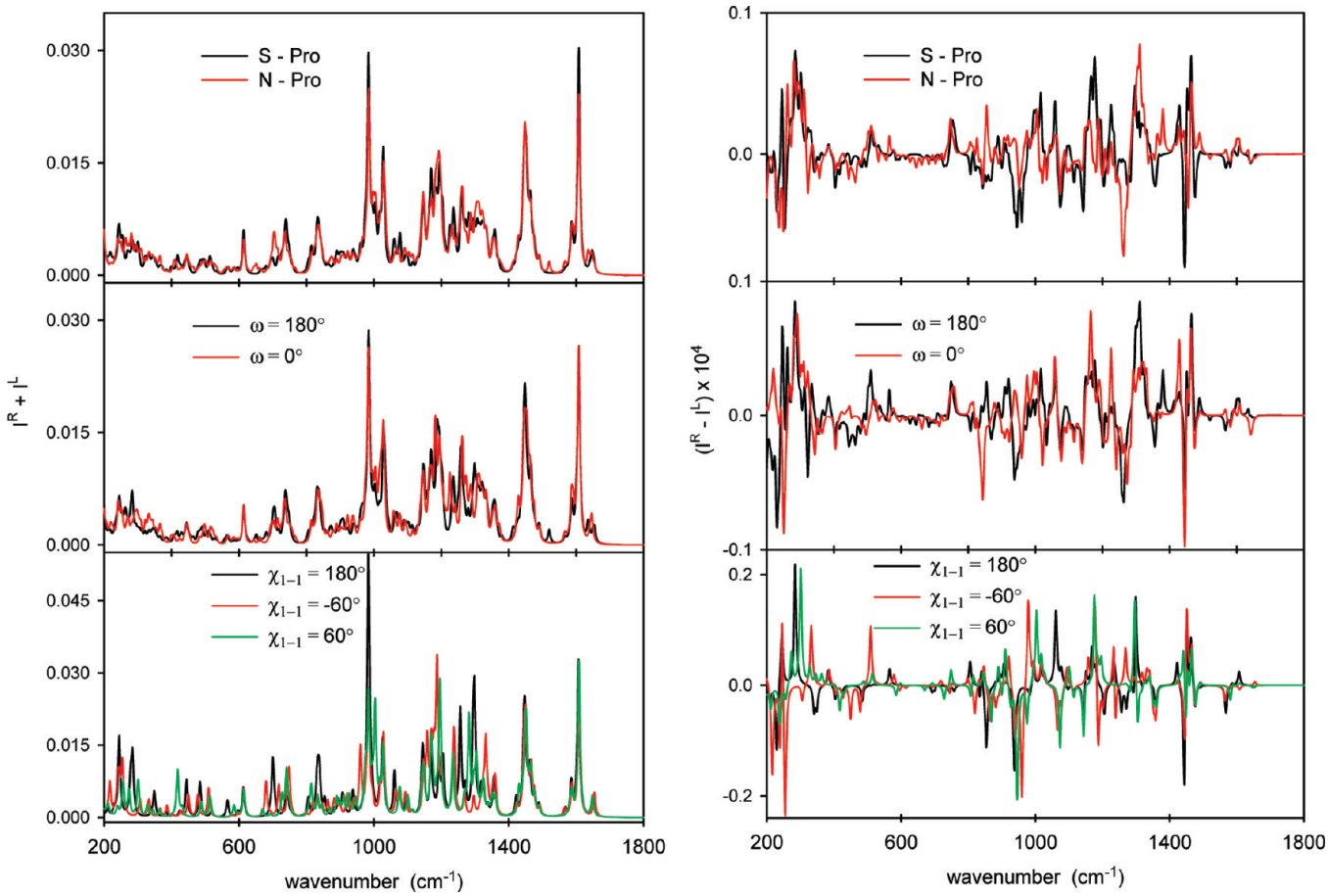

Figure 9. ROA spectra of the model Phe-D-Pro fragment simulated (BPW91/CPCM(H_2O)/6-31G**) for the different proline puckering and ω and χ_{1-1} angle values. The remaining coordinates were averaged with the conformers from Table 2.

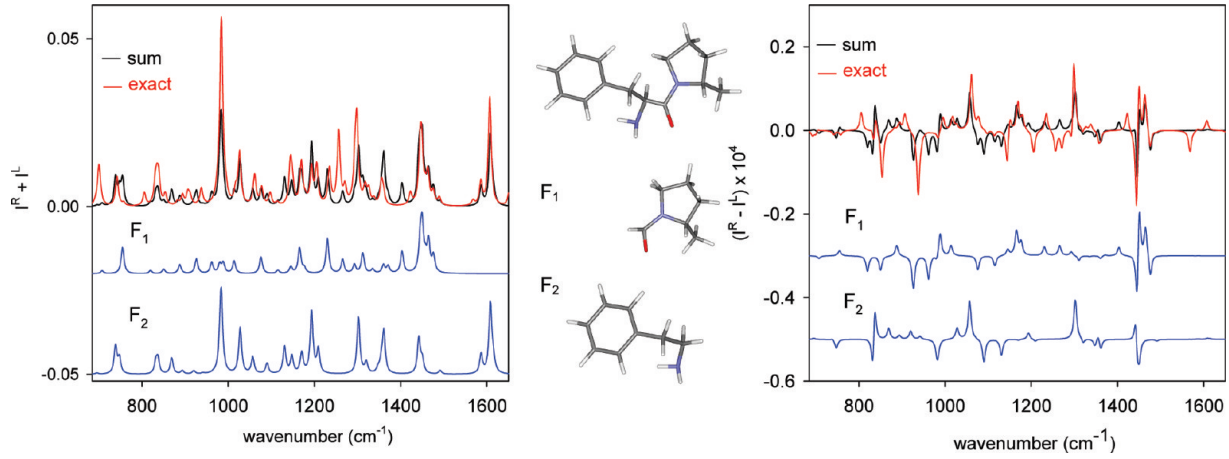

Figure 10. Calculated Raman (left) and ROA (right) Spectra of the Phe-D-Pro Fragment (top, red), and Its Two Phe and Pro Subfragments.

main ROA features within 1000−1500 cm^{-1} are unaffected, which again implies a local character for the ROA signal origin. Such observations have been made in the past and have shown aspects of the complementarity of IR and Raman, as well as VCD and ROA spectroscopies.[69] The largest changes are caused by the Phe residue χ_{1-1} rotation at the entire spectral region. This suggests a strong vibrational coupling between the achiral phenyl residue and the aliphatic CH_2 linkage. The ROA band at ∼1030 cm^{-1}, particularly sensitive to the χ_{1_1} rotation, is primarily caused by a breathing Phe vibration, with a minor contribution from Pro ring, and may well correspond to the negative experimental ROA band at 1152 cm^{-1}. This would correspond to χ_{1_1} values of ±60°, enabling a close interaction of the Pro and Phe hydrophobic residues that is quite probable in the aqueous environment. Indeed, the angular distribution obtained by the MD simulation (Figure 2) suggests that the angle of 180° is less probable than $\chi_{1-1} = 60°$.

To relate the local spectral signal of the Phe and Pro groups to the total in an alternate way, in the last computational experiment, we calculated Raman and ROA spectra of a Phe-D-Pro fragment and compared them to those obtained from two arbitrary subfragments (Figure 10). We can see that the influence of the inter-residue Phe-Pro coupling on ROA signal is rather small. Some bands (around 1200 cm^{-1}) are affected by the molecular division, but these originate in the covalent linkage (CH_2 bending, C−C stretching coupled with the amide modes).

The amide group contained in fragment F1 (Figure 10) does not have an obvious influence on ROA spectra. We can thus conclude that the ROA signal stems primarily from the intrinsic chirality of the peptide side chain residues rather than from interchain coupling interactions. The interactions, however, can change the conformation and thus modify the spectrum. Also, if the full peptide backbone is considered, the total contribution of the intergroup coupling to the resultant ROA signal is much larger (cf. Figure 6).

Conclusions

The Raman and ROA spectra of the hexapeptide provided useful complementary information about the structure and flexibility to that obtained from IR and VCD spectroscopy. The side chain residues were found to dominate the signal, in particular the Phe phenyl ring. Molecular dynamics simulations indicated that most side chain residues almost freely rotate between several preferred positions, which led to a specific broadening of Raman spectral lines and a significant (∼80%) decrease of the averaged ROA intensities. The averaging provided a dramatic improvement in simulated spectral line shapes, in comparison with a one conformer model. The polarization model suggested that the ROA intensity is primarily given by electric polarizability contributions and that the irreducible magnetic and quadrupolar parts are minor, although their inclusion in the analytical schemes does not complicate the computations, unlike for the previous numerical protocols. The majority of the ROA signal comes from locally chiral side chains, whereas the interchain coupling contribution was found to be limited. Many spectral features of the hexapeptide could be related to simpler theoretical and experimental dipeptide (Phe-D-Pro) models. The combination of the Raman and ROA spectroscopy with the multiscale computational technique thus brings extended information about biologically relevant molecules. Future instrumental and computational improvements are nevertheless desirable to investigate further details in molecular structure and dynamics.

Acknowledgment. The work was supported by the Grant Agency of the Czech Republic (Grants 203/06/0420, 202/07/0732), the Grant Agency of the Academy of Sciences (A400550702, M200550902), and the Grant Agency of Charles University (126310). The aspect of this work in Chicago was partially funded by the National Science Foundation (CHE07-18543) and that in Louisiana by a grant from the Petroleum Research Fund administered by the ACS (42027-AC4).

References and Notes

(1) Pančoška, P.; Frič, I.; Bláha, K. *Collect. Czech. Chem. Commun.* **1979**, *44*, 1296.
(2) Provencher, S. W.; Glockner, J. *Biochemistry* **1981**, *20*, 33.
(3) Johnson, W. C. *Proteins* **1990**, *7*, 205.
(4) Roy, A.; Bouř, P.; Keiderling, T. A. *Chirality* **2009**, *21*, E163.
(5) Keiderling, T. A. Conformational Studies of Proteins using Vibrational Circular Dichroism. In *Proteins: Structure, Dynamics, Design*; Renugopalakrishnan, V., Carey, P. R., Smith, I. C. P., Guang, S. G., Storer, A. C., Eds.; ESCOMP: Leiden, 1991; 165 pp.
(6) Bouř, P.; Keiderling, T. A. *J. Am. Chem. Soc.* **1993**, *115*, 9602.
(7) *Circular Dichroism Principles and Applications*; Berova, N., Nakanishi, K., Woody, R. W., Eds.; Wiley-VCH: New York, 2000.
(8) Keiderling, T. A. *Curr. Opin. Chem. Biol.* **2002**, *6*, 682.
(9) Barron, L. D.; Hecht, L.; Bell, A. D. Vibrational Raman Optical Activity of Biomolecules. In *Circular Dichroism and the Conformational Analysis of Biomolecules*; Fasman, G. D., Ed.; Plenum: New York, 1996; 653 pp.
(10) Barron, L. D.; Zhu, F.; Hecht, L.; Tranter, G. E.; Isaacs, N. W. *J. Mol. Struct.* **2007**, *834*−*836*, 7.
(11) Barron, L. D.; Zhu, F.; Hecht, L. *Vib. Spectrosc.* **2006**, *42*, 15.
(12) Keiderling, T. A.; Kubelka, J.; Hilario, J. Vibrational circular dichroism of biopolymers. Summary of methods and applications. In *Vibrational spectroscopy of polymers and biological systems*; Braiman, M., Gregoriou, V., Eds.; CRC Press: Boca Raton, FL, 2006; 253 pp.
(13) Silva, R. A. G. D.; Kubelka, J.; Decatur, S. M.; Bouř, P.; Keiderling, T. A. *Proc. Natl. Acad. Sci. U.S.A.* **2000**, *97*, 8318.
(14) Huang, R.; Setnička, V.; Etienne, M. A.; Kim, J.; Kubelka, J.; Hammer, R. P.; Keiderling, T. A. *J. Am. Chem. Soc.* **2007**, *129*, 13592.
(15) Hauser, K.; Krejtschi, C.; Huang, R.; Wu, L.; Keiderling, T. A. *J. Am. Chem. Soc.* **2008**, 2984.
(16) Huang, R.; Wu, L.; McElheny, D.; Bouř, P.; Roy, A.; Keiderling, T. A. 2009.
(17) Millhauser, G. L.; Stenland, C. J.; Hanson, P.; Bolin, K. A.; van de Ven, F. J. *J. Mol. Biol.* **1997**, *267*, 963.
(18) Silva, R. A. G. D.; Yasui, S.; Kubelka, J.; Formaggio, F.; Crisma, M.; Toniolo, C.; Keiderling, T. A. *Biopolymers* **2002**, *65*, 299.
(19) Dukor, R. K.; Keiderling, T. A.; Gut, V. *Int. J. Pept. Protein Res.* **1991**, *38*, 198.
(20) Yang, W. Y.; Pitera, J. W.; Swope, W. C.; Gruebele, M. *J. Mol. Biol.* **2004**, *336*, 241.
(21) Cochran, A. G.; Skelton, N. J.; Starovasnik, M. A. *Proc. Nat. Acad. Sci. U.S.A.* **2001**, *98*, 5578.
(22) Espinosa, J. F.; Gellman, S. H. *Angew. Chem., Int. Ed.* **2000**, *39*, 2330.
(23) Hilario, J.; Kubelka, J.; Syud, F. A.; Gellman, S. H.; Keiderling, T. A. *Biospectroscopy* **2002**, *67*, 233.
(24) Mantsch, H. H.; Perczel, A.; Hollosi, M.; Fasman, G. D. *Biopolymers* **1993**, *33*, 201.
(25) Vass, E.; Lang, E.; Samu, J.; Majer, Z.; Kajtar-Peredy, M.; Mak, M.; Radics., I.; Hollosi, M. *J. Mol. Struct.* **1998**, *440*, 59.
(26) Bouř, P.; Kim, J.; Kapitán, J.; Hamer, R. P.; Juany, R.; Wu, L.; Keiderling, T. A. *Chirality* **2008**, *20*, 1104.
(27) Buděšínský, M.; Šebestík, J.; Bednárová, L.; Baumruk, V.; Šafařík, M.; Bouř, P. *J. Org. Chem.* **2008**, *73*, 1481.
(28) Kapitán, J.; Baumruk, V.; Kopecký, V., Jr.; Bouř, P. *J. Phys. Chem. A* **2006**, *110*, 4689.
(29) Kapitán, J.; Johannessen, C.; Bouř, P.; Hecht, L.; Barron, L. D. *Chirality* **2009**, *21*, E4.
(30) Polavarapu, P. L.; Hecht, L.; Barron, L. D. *J. Phys. Chem.* **1993**, *97*, 1793.
(31) Ruud, K.; Helgaker, T.; Bouř, P. *J. Phys. Chem. A* **2002**, *106*, 7448.
(32) Liegeois, V.; Ruud, K.; Champagne, B. *J. Chem. Phys.* **2007**, *127*, 204105.
(33) Cheeseman, J. R., *Calculation of molecular chiroptical properties using density functional theory; CD 2007*, Groningen, 2007.
(34) Bouř, P.; Sopková, J.; Bednárová, L.; Maloň, P.; Keiderling, T. A. *J. Comput. Chem.* **1997**, *18*, 646.
(35) Kaminský, J.; Kapitán, J.; Baumruk, V.; Bednárová, L.; Bouř, P. *J. Phys. Chem. A* **2009**, *113*, 3594.
(36) Barany, G.; Albericio, F. *J. Am. Chem. Soc.* **1985**, *107*, 4936.
(37) Kates, S. A.; Sole, N. A.; Johnson, C. R.; Hudson, D.; Barany, G.; Albericio, F. *Tetrahedron Lett.* **1993**, *34*, 1549.
(38) Hanzlíková, J.; Praus, P.; Baumruk, V. *J. Mol. Struct.* **1999**, *481*, 431.
(39) Ponder, J. W. *Tinker, Software Tools for Molecular Design, 3.8 ed.*; Washington University School of Medicine: Saint Louis, MO, 2000.
(40) Cornell, W. D.; Cieplak, P.; Bayly, C. I.; Gould, I. R.; Merz, K. M.; Ferguson, D. M.; Spellmeyer, D. C.; Fox, T.; Caldwell, J. W.; Kollman, P. A. *J. Am. Chem. Soc.* **1995**, *117*, 5179.
(41) Kamiya, N.; Watanabe, Y. S.; Ono, S.; Higo, J. *Chem. Phys. Lett.* **2005**, *401*, 312.
(42) Frisch, M. J.; Trucks, G. W.; Schlegel, H. B.; Scuseria, G. E.; Robb, M. A.; Cheeseman, J. R.; Montgomery, J. A., Jr.; Vreven, T.; Kudin, K. N.; Burant, J. C.; Millam, J. M.; Iyengar, S. S.; Tomasi, J.; Barone, V.; Mennucci, B.; Cossi, M.; Scalmani, G.; Rega, N.; Petersson, G. A.; Nakatsuji, H.; Hada, M.; Ehara, M.; Toyota, K.; Fukuda, R.; Hasegawa, J.; Ishida, M.; Nakajima, T.; Honda, Y.; Kitao, O.; Nakai, H.; Klene, M.; Li, X.; Knox, J. E.; Hratchian, H. P.; Cross, J. B.; Bakken, V.; Adamo, C.; Jaramillo, J.; Gomperts, R.; Stratmann, R. E.; Yazyev, O.; Austin, A. J.; Cammi, R.; Pomelli, C.; Ochterski, J. W.; Ayala, P. Y.; Morokuma, K.; Voth, G. A.; Salvador, P.; Dannenberg, J. J.; Zakrzewski, V. G.; Dapprich, S.; Daniels, A. D.; Strain, M. C.; Farkas, O.; Malick, D. K.; Rabuck, A. D.; Raghavachari, K.; Foresman, J. B.; Ortiz, J. V.; Cui, Q.; Baboul, A. G.; Clifford, S.; Cioslowski, J.; Stefanov, B. B.; Liu, G.; Liashenko, A.; Piskorz, P.; Komaromi, I.; Martin, R. L.; Fox, D. J.; Keith, T.; Al-Laham, M. A.; Peng, C. Y.; Nanayakkara, A.; Challacombe, M.; Gill, P. M. W.; Johnson, B.; Chen, W.; Wong, M. W.; Gonzalez, C.; Pople, J. A. *Gaussian 03, Revision C.02*; Gaussian, Inc.: Wallingford, CT, 2004.
(43) Frisch, M. J.; Trucks, G. W.; Schlegel, H. B.; Scuseria, G. E.; Robb, M. A.; Cheeseman, J. R.; Scalmani, G.; Barone, V.; Mennucci, B.; Petersson, G. A.; Nakatsuji, H.; Caricato, M.; Li, X.; Hratchian, H. P.; Izmaylov, A. F.; Bloino, J.; Zheng, G.; Sonnenberg, J. L.; Hada, M.; Ehara, M.; Toyota, K.; Fukuda, R.; Hasegawa, J.; Ishida, M.; Nakajima, T.; Honda, Y.; Kitao, O.;

Nakai, H.; Vreven, T.; Montgomery, J., J. A.; Peralta, J. E.; Ogliaro, F.; Bearpark, M.; Heyd, J. J.; Brothers, E.; Kudin, K. N.; Staroverov, V. N.; Kobayashi, R.; Normand, J.; Raghavachari, K.; Rendell, A.; Burant, J. C.; Iyengar, S. S.; Tomasi, J.; Cossi, M.; Rega, N.; Millam, J. M.; Klene, M.; Knox, J. E.; Cross, J. B.; Bakken, V.; Adamo, C.; Jaramillo, J.; Gomperts, R.; Stratmann, R. E.; Yazyev, O.; Austin, A. J.; Cammi, R.; Pomelli, C.; Ochterski, J. W.; Martin, R. L.; Morokuma, K.; Zakrzewski, V. G.; Voth, G. A.; Salvador, P.; Dannenberg, J. J.; Dapprich, S.; Daniels, A. D.; Farkas, O.; Foresman, J. B.; Ortiz, J. V.; Cioslowski, J.; Fox, D. J. *Gaussian 09, Revision A.02*; Gaussian, Inc.: Wallingford, CT, 2009.

(44) Bouř, P.; Keiderling, T. A. *J. Chem. Phys.* **2002**, *117*, 4126.

(45) Bouř, P. *Collect. Czech. Chem. Commun.* **2005**, *70*, 1315.

(46) Barron, L. D. *Molecular Light Scattering and Optical Activity*; Cambridge University Press: Cambridge, 2004.

(47) Becke, A. *Phys. Rev. A* **1988**, *38*, 3098.

(48) Becke, A. D. *J. Chem. Phys.* **1993**, *98*, 5648.

(49) Klamt, A. COSMO and COSMO-RS. In *The Encyclopedia of Computational Chemistry*; Schleyer, P. R., Allinger, N. L., Clark, T., Gasteiger, J., Kollman, P. A., Schaefer, H. F., III, Schreiner, P. R., Eds.; John Wiley & Sons: Chichester, 1998; Vol. 1, 604 pp.

(50) Polavarapu, P. L. *Vib. Spectra Struct.* **1984**, *13*, 103.

(51) Daněček, P.; Kapitán, J.; Baumruk, V.; Bednárová, L.; Kopecký, V., Jr.; Bouř, P. *J. Chem. Phys.* **2007**, *126*, 224513.

(52) Zuber, G.; Hug, W. *J. Phys. Chem. A* **2004**, *108*, 2108.

(53) Reiher, M.; Liegeois, V.; Ruud, K. *J. Phys. Chem. A* **2005**, *109*, 7567.

(54) Šebek, J.; Kapitán, J.; Šebestík, J.; Baumruk, V.; Bouř, P. *J. Phys. Chem. A* **2009**, *113*, 7760.

(55) Kapitán, J.; Baumruk, V.; Kopecký, V., Jr.; Pohl, R.; Bouř, P. *J. Am. Chem. Soc.* **2006**, *128*, 13451.

(56) Jalkanen, K. J.; Nieminen, R. M.; Frimand, K.; Bohr, J.; Bohr, H.; Wade, R. C.; Tajkhorshid, E.; Suhai, S. *Chem. Phys.* **2001**, *265*, 125.

(57) Bouř, P.; Keiderling, T. A. *J. Phys. Chem. B* **2005**, *109*, 5348.

(58) Kubelka, J.; Huang, R.; Keiderling, T. A. *J. Phys. Chem. B* **2005**, *109*, 8231.

(59) Bouř, P.; Baumruk, V.; Hanzlíková, J. *Collect. Czech. Chem. Commun.* **1997**, *62*, 1384.

(60) Bouř, P. *J. Comput. Chem.* **2001**, *22*, 426.

(61) Kapitán, J.; Baumruk, V.; Kopecký, V., Jr.; Bouř, P. *J. Am. Chem. Soc.* **2006**, *128*, 2438.

(62) Buděšínský, M.; Daněček, P.; Bednárová, L.; Kapitán, J.; Baumruk, V.; Bouř, P. *J. Phys. Chem. A* **2008**, *112*, 8633.

(63) Bouř, P.; Raich, I.; Kaminský, J.; Hrabal, R.; Čejka, J.; Sychrovský, V. *J. Phys. Chem. A* **2004**, *108*, 6365.

(64) Altona, C.; Sundaralingam, M. *J. Am. Chem. Soc.* **1972**, *94*, 8205.

(65) Kang, Y. K.; Park, H. S. *J. Mol. Struct. (THEOCHEM)* **2005**, *718*, 17.

(66) Kang, Y. K. *J. Phys. Chem. B* **2004**, *108*, 5463.

(67) Kang, Y. K.; Choi, H. Y. *Biophys. Chem.* **2004**, *11*, 135.

(68) Song, I. K.; Kang, Y. K. *J. Phys. Chem. B* **2005**, *109*, 16982.

(69) Tam, C. N.; Bouř, P.; Keiderling, T. A. *J. Am. Chem. Soc.* **1997**, *119*, 7061.

JP104744A